Theoretical Investigation of the $H_3O^+(H_2O)_4$ Cluster

R. A. Christie and K. D. Jordan*

Department of Chemistry and Center for Molecular and Materials Simulations, University of Pittsburgh, Pittsburgh, Pennsylvania 15260

Received: April 2, 2001

The low-lying minima on the Born−Oppenheimer potential energy surface of the $H_3O^+(H_2O)_4$ cluster are investigated by effective valence bond (EVB), density functional, and MP2 methods. Although Becke3LYP and MP2 calculations predict the same global minimum structure, the relative energies of various structures obtained by these two approaches differ by up to 1.7 kcal/mol. Even larger differences are found between the relative energies calculated at the EVB and MP2 levels of theory. Vibrational spectra are calculated for each of the minimum energy species.

I. Introduction

Small protonated water clusters have been the subject of numerous theoretical studies.[1−20] Although the Born−Oppenheimer potential energy surface for the $H_3O^+(H_2O)_n$, $n = 1-3$, clusters are fairly well characterized, much less is known about the larger protonated water clusters. In this work, we consider the $H_3O^+(H_2O)_4$ system, which is of particular interest in that it is the smallest protonated water cluster with a water molecule outside the first solvation shell of H_3O^+.[1] The perturbation of the first solvation shell by surrounding solvent molecules is a vital phenomenon in aqueous phase chemistry and biology, and has been invoked to account for the anomalously high rate of proton transfer in bulk water.[13]

In this study, five potential energy minima of $H_3O^+(H_2O)_4$ (see Figure 1) have been characterized. Four of these (**I**, **II**, **IV**, and **V**) were considered in earlier theoretical studies.[17,18] Species **III** is reported here for the first time. In isomers **I**, **II**, and **III** the H_3O^+ entity is directly bonded to three water monomers, and in **IV** and **V**, it is bonded to two water monomers. **I**−**III** can be viewed as Eigen-like[21] $H_9O_4^+$ ions solvated by an additional water monomer. In **I**, the H_3O^+ is incorporated into a four-membered ring and is bonded to two waters in the ring as well as to a nonring water. **II** and **III**, which may be viewed as an $H_9O_4^+$ ion solvated by a H_2O molecule, can interconvert by inversion of the central H_3O^+ species. **IV** is a chainlike structure with the H_3O^+ located in the middle of the chain, and **V** has a five-membered ring structure.

The most thorough earlier theoretical studies of $H_3O^+(H_2O)_4$ are those of Hodges and Stone[17] and Corongiu et al.[18] Whereas Hodges and Stone employed a model potential to describe the cluster, Corongiu et al.[18] used density functional theory (DFT) with the Becke−Perdew (BP) exchange correlation functional[22−24] Both of these approaches predict the global minimum structure to be **I**, with the next most stable structure (**II**) lying about 1.5 kcal/mol higher in energy. The relative stabilities predicted by these calculations cannot be viewed as conclusive as the BP functional used by Corongiu et al.[18] considerably overestimates H-bond strengths in water clusters[25−28] and the model potential of Hodges and Stone employs a rigid H_3O^+ entity.

In the present work, three additional theoretical methods are brought to bear on the $H_3O^+(H_2O)_4$ system. These include second-order many-body perturbation theory (MP2), density functional theory with the Becke3LYP exchange-correlation functional[29−31] and the multistate empirical valence bond (MSEVB) approach of Schmitt and Voth.[16] Previous studies have proven that the MP2 method allows an accurate characterization of smaller $H_3O^+(H_2O)_n$ clusters.[8,9,32] Hence, comparison with the MP2 results will prove valuable in assessing the reliability of the Hodges-Stone[17] and MSEVB model potential approaches as well as of the BP and Becke3LYP density functional methods for describing $H_3O^+(H_2O)_4$ and larger protonated water clusters.

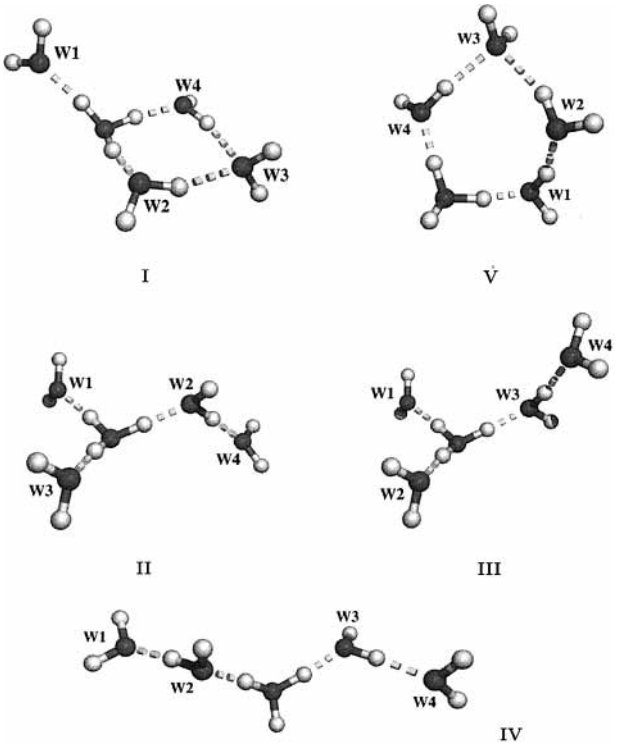

Figure 1. MP2/aug-cc-pVDZ optimized geometrical structures of $H_3O^+(H_2O)_4$.

II. Methodology

The geometries of the clusters were first optimized using the MSEVB[16] method, combined with a Monte Carlo quenching

10.1021/jp011241b CCC: $20.00
Published on Web 07/26/2001

TABLE 1: Comparison of Formation Energies (kcal/mol) for the Five $H_3O^+(H_2O)_4$ Minima Calculated Using Various Theoretical Methods[a]

isomer	MP2/aDZ[b] at MP2	MP2/aTZ[b] at MP2	MP2/aDZ at B3LYP	B3LYP/aDZ at B3LYP	BP[c]	BP86/aDZ at B3LYP	MSEVB	Hodges Stone[d]	MP2/aDZ at MSEVB
I	−92.71	−92.60	−92.67	−91.71	−97.04	−91.56	−91.08	−85.88	−90.54
II	−91.53	−91.72	−91.43	−91.67	−95.36	−91.71	−92.07	−84.43	−89.48
III	−91.58	−91.74	−91.48	−91.63		−91.74	−92.01		−89.61
IV	−88.03	−88.47	−87.89	−88.76	−92.74	−89.68	−83.96		−85.26
V	−88.44	−88.60	−88.27	−87.84	−94.42	−88.53	−85.37	−83.71	−86.77

[a] For those entries with two theoretical methods listed, the first method refers to that used to calculate the energy and the second to the method at which the geometry was optimized. The MP2 and Becke3LYP geometries were optimized using the aug-cc-pVDZ basis set. [b] aDZ and aTZ denote the aug-cc-pVDZ and aug-cc-pVTZ basis sets, respectively. [c] From ref 18. [d] From ref 17.

TABLE 2: *n*-body Contributions to the MP2 Formation Energies (kcal/mol) for I, II, IV, and V

	I		II		IV		V	
interaction	aDZ[a]	aTZ[a]	aDZ	aTZ	aDZ	aTZ	aDZ	aTZ
1-body	2.39	2.89	2.88	3.36	6.90	7.60	6.73	7.45
2-body	−107.06	−107.56	−103.81	−104.49	−92.99	−94.19	−96.51	−97.39
	(−100.71)[b]	(−104.41)	(−97.89)	(−101.62)	(−86.81)	(−91.10)	(−89.59)	(−93.91)
3-body	11.59	11.69	9.39	9.36	−3.09	−3.00	0.10	0.12
	(11.69)	(11.71)	(9.47)	(9.44)	(−2.93)	(−2.94)	(0.10)	(0.15)
4-body	0.44	0.43	0.03	0.08	1.13	1.09	1.18	1.19
	(0.41)	(0.42)	(0.07)	(0.07)	(1.07)	(1.07)	(1.14)	(1.13)
5-body	−0.07	−0.05	−0.02	−0.03	0.02	0.03	0.06	0.03
	(−0.05)	(−0.05)	(−0.03)	(−0.03)	(0.02)	(0.03)	(0.05)	(0.05)
net	−92.71	−92.60	−91.53	−91.72	−88.03	−88.47	−88.44	−88.60
	(−86.27)	(−89.44)	(−85.50)	(−88.78)	(−81.75)	(−85.34)	(−81.57)	(−85.13)

[a] The aug-cc-pVDZ and aug-cc-pVTZ basis sets are denoted aDZ and aTZ, respectively. [b] Terms in parentheses correspond to the counterpoise-corrected values.

procedure. The MSEVB approach has been described in detail in ref 16, and here, we note only that it combines a modified nonrigid monomer TIP3P[33] model potential for describing the $H_2O\cdots H_2O$ interactions and a parametrized valence bond treatment of the $H_3O^+\cdots H_2O$ interactions. Starting from the MSEVB structures, the geometries were then optimized at both the Becke3LYP and MP2 levels of theory using the aug-cc-pVDZ basis set.[34,35]

To determine whether differences in the relative energies obtained at the Becke3LYP and MP2 levels of theory were due to the differences in the geometries, single-point MP2/aug-cc-pVDZ calculations were carried out at the Becke3LYP potential energy minima. To check the convergence of the results with the respect to the atomic basis set, MP2 calculations were carried out using the larger aug-cc-pVTZ basis set.[34,35]

As is well known, basis set superposition error (BSSE) can cause interaction energies to be overestimated. Corrections for BSSE have been estimated by use of the counterpoise procedure.[36] To obtain insight into the nature of the interactions for each cluster, the net MP2 interaction energies were decomposed into their *n*-body ($n = 2$, 3, 4 and 5) contributions. This was accomplished by carrying out calculations on appropriate fragment combinations as will be described in more detail below.

The relative energies obtained from the Becke3LYP/aug-cc-pVDZ calculations were found to differ appreciably from the BP results of Corongiu et al.[18] However there are two major differences between these two DFT calculations: (1) the exchange-correlation functionals differ, and (2) the basis set used for our calculations contains diffuse functions, whereas that used by Corongiu et al.[18] did not. To determine which of these two factors is responsible for the discrepancies between the two sets of DFT results, we also undertook BP calculations using both the cc-pVDZ basis set which lacks diffuse functions and the aug-cc-pVDZ basis set which includes such functions. These calculations were carried out using the Becke3LYP optimized geometries. Finally, the IR spectra were calculated for isomers **I**, **II**, **IV**, and **V** using the harmonic approximation and the Becke3LYP/aug-cc-pVDZ procedure.

The electronic structure calculations were performed with the Gaussian 98 program,[31] and the MSEVB calculations were carried out using a program developed in our group.

III. Results and Discussion

(i) Energies of the Isomers I−V. Table 1 summarizes the formation energies for the different isomers calculated at the various levels of theory. A subset of the results is also summarized in Figure 1. The formation energies are calculated using

$$\Delta E = E(H_3O^+(H_2O)_4) - E(H_3O^+) - 4\cdot E(H_2O) \quad (1)$$

where $E(H_3O^+(H_2O)_4)$, $E(H_3O^+)$, and $E(H_2O)$ are the energies of the $H_3O^+(H_2O)_4$ cluster, the H_3O^+ ion, and the H_2O molecule, respectively.

The MP2/aug-cc-pVDZ calculations predict that **I** is the global minimum structure, lying energetically about 1.2 kcal/mol below the nearly isoenergetic minima **II** and **III**. At the MP2 level of theory, **IV** and **V** are predicted to be less stable than **I** by 4.68 and 4.27 kcal/mol, respectively.

The formation energies calculated at the MP2/aug-cc-pVTZ level are very close to those obtained at the MP2/aug-cc-pVDZ level, both without correction for BSSE. However, the counterpoise corrections for the BSSE in the MP2 formation energies range from 5.9 to 6.9 kcal/mol with the aug-cc-pVDZ basis set and from 2.9 to 3.5 kcal/mol with the aug-cc-pVTZ basis set (see Table 2). On the basis of the trends in Table 2, and on the results for neutral water clusters employing still larger basis sets, we expect the complete basis set (CBS) limit MP2 level formation energies to be very close to the uncorrected MP2/aug-cc-pVTZ results. For this reason, unless noted otherwise, in assessing the reliability of the DFT and MSEVB results, comparison will be made with the MP2/aug-cc-pVTZ results.

For **II**, **III**, and **IV**, the Becke3LYP and MP2 calculations give similar formation energies. However, for **I** and **V**, the Becke3LYP calculations give formation energies 0.8−0.9 kcal/mol smaller in magnitude than the corresponding MP2 values. As a result, the Becke3LYP calculations predict minima **II** and **III** to be nearly isoenergetic with **I** and predict **IV** to be more stable than **V**, in contrast with the MP2 results. Interestingly, of the five isomers of $H_9O_4^+$, only **I** and **V** have a double-acceptor water monomer. Thus, it appears that the Becke3LYP functional is inadequate for describing the interactions involving double-acceptor water molecules. This is consistent with an earlier observation that for $(H_2O)_6$, Becke3LYP calculations incorrectly predict the ring isomer to be more stable than the cage and prism isomers, both of which have double acceptor water molecules.[37] This problem is not unique to the Becke3LYP functional, as similar behavior is also displayed by BP/aug-cc-pVDZ calculations.

At the Becke3LYP/aug-cc-pVDZ level the inversion barrier of **III** is 0.47 kcal/mol, nearly identical to that (0.52 kcal/mol) for the $H_9O_4^+$ Eigen-like ion. In contrast, the inversion barrier (at the same level of theory) for H_3O^+ is 1.36 kcal/mol.

As is seen from the results in Table 1 and Figure 1, although the BP calculations of Corongiu et al.[18] predict **I** to be the global minimum form of $H_3O^+(H_2O)_4$ in agreement with our MP2 calculations, this agreement is fortuitous, being the result of the use of a basis set lacking diffuse functions. BP calculations with the aug-cc-pVDZ basis set, in fact, predict **II** and **III** to be about 0.2 kcal/mol more stable than **I**.

MP2 calculations using Becke3LYP optimized geometries give relative energies for the different isomers nearly identical to those obtained using MP2 optimized geometries, which is not surprising given that the formation energies from the Becke3LYP calculations are fairly close to the MP2 results.

With the inclusion of counterpoise corrections (Table 2), **I** is predicted, at the MP2/aug-cc-pVTZ level, to be more stable (by $\approx$ 0.7 kcal/mol) than **II**/**III**. The vibrational zero-point energy (calculated using Becke3LYP/aug-cc-pVDZ harmonic frequencies) for **I** is 9.0 kcal/mol, but only about 7.6 to 7.8 kcal/mol for **II** and **III**. When the MP2/aug-cc-pVTZ level formation energies are combined with the B3LYP/aug-cc-pVDZ ZPE corrections, **II** and **III** are predicted to be slightly more stable than **I**.

We now turn our attention to the model potential results. Although the Hodges and Stone (HS) potential underestimates the formation energies by up to about 7.3 kcal/mol, it does a fairly good job at reproducing the relative stabilities obtained at the MP2 level. Presumably, with a more exhaustive search for local minima, isomers **III** and **IV** would be identified for this potential.

The MSEVB calculations, in contrast to the MP2 calculations, place structures **II** and **III** below **I** (by about 1.0 kcal/mol). They also place **IV** and **V** 3−5 kcal/mol too high in energy, which seems to imply that the MSEVB procedure is biased toward a fully solvated over a partially solvated H_3O^+ ion. We return to this issue in the next section where the individual *n*-body contributions to the formation energies are examined.

MP2 calculations carried out using the MSEVB geometries underestimate the magnitude of the formation energies by up to 1.8−3.2 kcal/mol (as compared to the results obtained using the MP2 or Becke3LYP optimized geometries). The approximate near constancy of the error introduced by the use of the MSEVB geometries is an encouraging finding as it is much less computationally demanding to optimize structures at the MSEVB than at the MP2 (or Becke3LYP) level of theory.

To elucidate the effect of the secondary solvation shell molecule upon the relative energies, it is instructive to compare the results for the $H_3O^+(H_2O)_4$ cluster with those for the $H_3O^+(H_2O)_3$. To this end, the $H_3O^+(H_2O)_3$ species, **I′**, **II′**, and **IV′**, were optimized at the MP2/aug-cc-pVDZ level of theory. The three unique $H_3O^+(H_2O)_3$ isomers obtained are illustrated in Figure 6. **I′** corresponds to minima **I** without the **W1** H_2O monomer (see Figure 1). **II′** is formed by removing the secondary shell water molecule (**W4** in Figure 1) from **II** to leave the Eigen cation. **IV′** corresponds to **IV** with one of the terminal H_2O monomers (**W1** or **W4**) removed. For the $H_3O^+(H_2O)_3$ cluster, the Eigen cation **II′** is predicted to be 4.0 kcal/mol more stable than **I′**. This is in contrast to $H_3O^+(H_2O)_4$ for which **I** is predicted to be more stable than **II**. The reversal of the order of these two structures upon addition of a water monomer is the result of the much greater strength of the $H_3O^+\cdots H_2O$ interaction compared to the $H_2O\cdots H_2O$ interaction (see Figure 4).

(ii) *n*-body Interaction Energies. The Becke3LYP, MP2, and MSEVB interaction energies were decomposed into their various *n*-body contributions.[37,38] This was accomplished by carrying out calculations on all possible cluster fragments. For example, to estimate the two-body interaction energies, calculations were carried out on each $H_3O^+\cdots H_2O$ and $H_2O\cdots H_2O$ pair, as well as on each monomer in the cluster, using the geometries "extracted" from that of the $H_3O^+(H_2O)_4$ isomer of interest. The two-body contributions to the interaction energies were then calculated by subtracting from the "dimer" energies the appropriate monomer energies. To obtain the three and four-body interaction energies calculations on all trimer and tetramer combinations were required. The *n*-body decomposition analysis was carried out using both the aug-cc-pVDZ and aug-cc-pVTZ basis sets in the case of the MP2 calculations, but only the aug-cc-pVDZ basis set in the case of the B3LYP calculations. MP2/aug-cc-pVDZ geometries were used in each case to remove differences caused by variations in the geometries from one theoretical approach to another.

The results of the *n*-body decomposition calculations are summarized in Tables 2−5. Interaction energies with and without the counterpoise correction for BSSE are reported. The table also reports 1-body relaxation energies which are the energies required to distort isolated H_3O^+ and H_2O species to the geometries they possess in the cluster. We examine first the results from the MP2 calculations summarized in Table 2. In the absence of the counterpoise correction, the individual *n*-body contributions, and consequently, the net interaction energies, are relatively independent of whether the aug-cc-pVDZ or aug-cc-pVTZ basis sets is employed. In particular, the $n \geq 3$ *n*-body interaction energies calculated with the aug-cc-pVDZ and aug-cc-pVTZ basis sets agree to within 0.1 kcal/mol. Counterpoise corrections to the $n \geq 3$ *n*-body interactions are found to be very small. However, they are sizable for the two-body interaction energies, ranging from 5.9 to 6.9 kcal/mol with the aug-cc-pVDZ basis set and from 2.9 to 3.5 kcal/mol with the aug-cc-pVTZ basis set. Thus, the relative insensitivity of the 2-body interaction energies (and, hence, the net binding energies) to the basis set is in part fortuitous, reflecting the opposing tendencies of the BSSE to decrease and the "true" binding energy to increase in magnitude with increasing basis set flexibilty. The complete-basis-set limit MP2 level 2-body interaction energies are expected to fall close to the uncorrected aug-cc-pVTZ results. This was confirmed by carrying out MP2/aug-cc-pVQZ[34,35] calculations of the two-body interaction energies for **I**-**V**. In each case, the resulting interaction energy

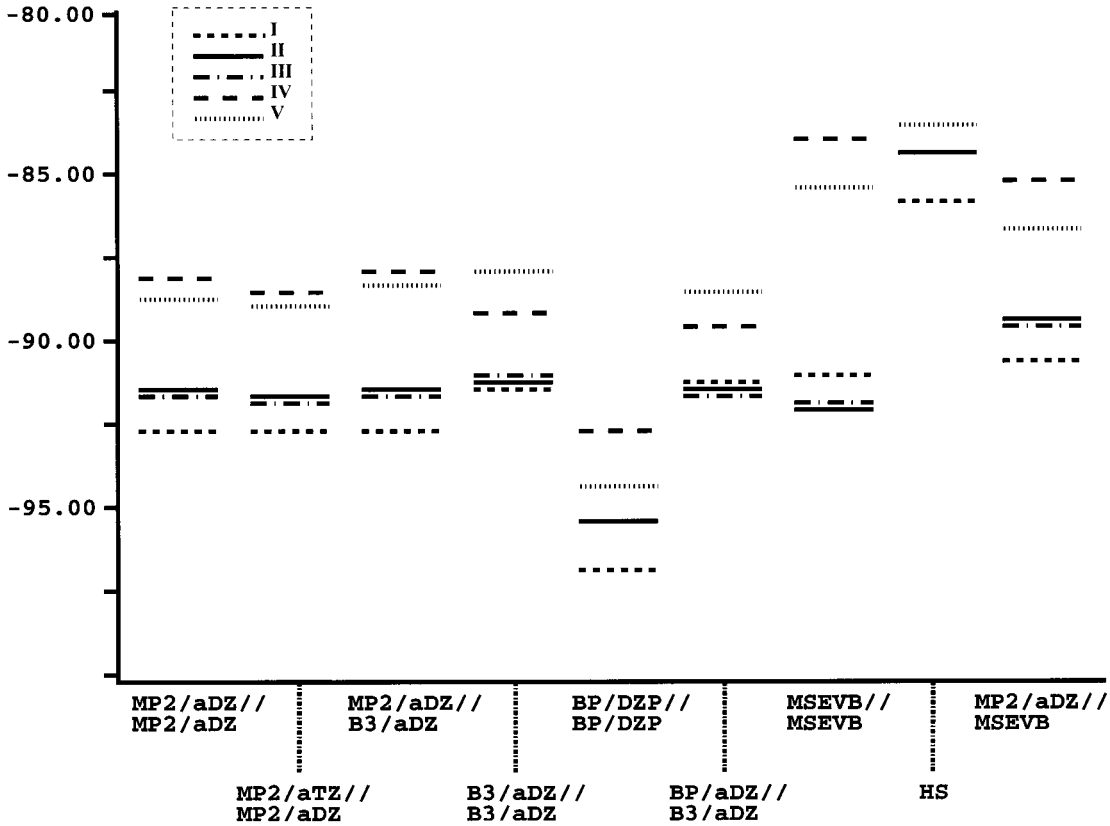

Figure 2. From left to right on absissca; MP2/aDZ//MP2/aDZ, MP2/aTZ//MP2/aDZ, MP2/aDZ//B3LYP/aDZ, B3LYP/aDZ//B3LYP/aDZ, BP/DZP//BP/DZP, BP86/aDZ//B3LYP/aDZ, MSEVB//MSEVB, HS//HS, and MP2/aDZ//MSEVB results respectively, where aDZ and aTZ denote aug-cc-pVDZ and aug-cc-pVTZ respectively, and where the quantity to the left of the double slash indicates the level of theory used to calculate the energies and that to the right, the geometries employed. HS denotes the model potential of Hodges and Stone,[17] and the BP/DZP//BP/DZP results are from Corongiu *et al.*[18]

TABLE 3: MP2/Aug-cc-pVTZ and MSEVB 2-body Interaction Energies (kcal/mol) for I, II, IV, and V

	I		II		IV		V	
2-body fragment[a]	MP2[b]	MSEVB[c]	MP2	MSEVB	MP2	MSEVB	MP2	MSEVB
H_3O^+,*W*1	−31.34	−31.91	−30.64	−31.10	−7.46	−6.20	−37.00	−41.55
H_3O^+,*W*2	−30.53	−31.93	−34.76	−34.92	−36.66	−39.99	−9.08	−6.41
H_3O^+,*W*3	−10.12	−8.92	−30.63	−31.03	−35.88	−32.16	−7.61	−6.32
H_3O^+,*W*4	−30.42	−29.80	−7.24	−5.83	−7.80	−5.42	−32.78	−30.78
W1,W2	0.87	1.49	0.77	1.57	−3.92	−7.14	−3.73	−6.86
W1,W3	0.35	0.62	0.75	1.54	0.33	0.51	−0.36	−0.36
W1,W4	0.71	1.47	0.29	0.54	0.14	0.21	0.87	1.45
W2,W3	−4.24	−4.62	0.73	1.51	0.77	1.53	−4.23	−5.09
W2,W4	1.44	2.72	−4.08	−7.27	0.29	0.32	1.15	2.34
W3,W4	−4.28	−4.04	0.32	0.44	−4.00	−7.48	−4.62	−5.39
sum of 2-body terms	−107.56	−104.92	−104.49	−104.55	−94.19	−95.82	−7.39	−98.97

[a] Numbering scheme for cluster fragments is depicted in Figure 1. [b] MP2/aug-cc-pVTZ energies calculated at MP2/aug-cc-pVDZ geometries. [c] MSEVB energies calculated at MP2/aug-cc-pVDZ geometries.

is found to agree to within 0.1 kcal/mol of the corresponding MP2/aug-cc-pVTZ result.

The trends discussed above for the $H_3O^+(H_2O)_4$ cluster are consistent with those reported previously by Pedulla et al.[37] for the neutral water clusters. In particular, in both cases, the $n \geq 3$ body interaction energies are relatively insensitive to the basis set, leading to the conclusion that the need for large basis sets to attain convergence in supermolecule calculations is due almost entirely to the 2-body (and 1-body) contributions to the interaction energies. This suggests that for protonated clusters (as for the neutral clusters) accurate formation energies can be obtained by combining MP2/aug-cc-pVTZ (or MP2/aug-cc-pVQZ) results for the 1- and 2-body interaction energies with MP2/aug-cc-pVDZ results for the higher-body interaction energies.

The net three-body interaction energies are calculated to range from 11.7 kcal/mol in **I** to −3.0 kcal/mol in **IV**. This is in contrast to the situation for the low energy structures of neutral water clusters, for which the net three-body terms are usually attractive.[37] The large variation in the three-body interaction energies in the $H_3O^+(H_2O)_4$ clusters is due to the fact that the H_3O^+ ion orientates the nearby H_2O monomers so that their dipoles are unfavorably aligned (with respect to the $H_2O\cdots H_2O$ interactions). When these water monomers are polarized by the H_3O^+ entity, their interactions with the other nearby water monomers become even less favorable. This is examined in more detail in Table 4 which lists the individual 3-body interaction energies of **I**, **II**, **IV**, and **V** calculated at the MP2/aug-cc-pVTZ level of theory. The table also lists results obtained using the MSEVB method which will be considered later in

TABLE 4: MP2/Aug-cc-pVTZ and MSEVB 3-body Interaction Energies (kcal/mol) for I, II, IV, and V

	I		II		IV		V	
3-body fragment[a]	MP2[b]	MSEVB[c]	MP2[b]	MSEVB[c]	MP2[b]	MSEVB[c]	MP2[b]	MSEVB[c]
H_3O^+,*W*1,*W*2	4.26	3.52	4.96	3.57	−6.50	−4.62	−4.83	−5.52
H_3O^+,*W*1,*W*3	0.91	0.17	3.94	2.52	0.83	0.14	0.28	−0.04
H_3O^+,*W*1,*W*4	4.37	2.76	0.57	0.12	0.10	0.00	6.88	6.03
H_3O^+,*W*2,*W*3	−1.94	−1.88	4.90	3.55	7.15	5.36	−0.06	0.00
H_3O^+,*W*2,*W*4	5.21	3.62	−5.89	−2.88	0.79	0.28	1.36	0.34
H_3O^+,*W*3,*W*4	−1.96	−1.16	0.60	0.12	−5.94	−1.90	−3.80	−1.42
W1,W2,W3	0.10	0.00	−0.07	0.00	0.24	0.00	−0.94	0.00
W1,W2,W4	−0.09	0.00	0.15	0.00	0.11	0.00	0.22	0.00
W1,W3,W4	0.04	0.00	−0.02	0.00	0.07	0.00	0.19	0.00
W2,W3,W4	0.79	0.00	0.22	0.00	0.15	0.00	0.82	0.00
sum of 3-body terms	11.69	7.03	9.36	7.00	−3.00	−0.74	0.12	−0.61

[a] Numbering scheme for cluster fragments is depicted in Figure 1. [b] MP2/aug-cc-pVTZ energies calculated at MP2/aug-cc-pVDZ geometries. [c] MSEVB energies calculated at MSEVB geometries.

TABLE 5: *n*-body Contributions to the Formation Energies (kcal/mol) for Minima I, II, IV and V Calculated at the MP2, B3LYP and MSEVB Levels of Theory

	I			II			IV			V		
interaction	MP2[a]	B3LYP[b]	MSEVB[c]	MP2	B3LYP	MSEVB	MP2	B3LYP	MSEVB	MP2	B3LYP	MSEVB
1-body	2.89	2.37	8.35	3.36	2.63	6.19	7.60	6.55	10.40	7.45	6.55	12.57
2-body	−107.56	−106.66	−104.92	−104.49	−104.20	−104.55	−94.19	−92.95	−95.82	−97.39	−95.26	−98.97
3-body	11.69	12.78	7.03	9.36	10.59	7.00	−3.00	−2.95	−0.74	0.12	0.27	−0.61
4-body	0.43	0.38	−1.44	0.08	−0.11	−0.42	1.09	0.95	2.10	1.19	0.96	1.76
5-body	−0.05	−0.21	−0.l0	−0.03	−0.21	−0.29	0.03	−0.14	0.10	0.03	0.16	−0.12

[a] MP2/aug-cc-pVTZ energies calculated using MP2/aug-cc-pVDZ geometries. [b] B3LYP/aug-cc-pVDZ energies calculated using MP2/aug-cc-pVDZ geometries. [c] MSEVB energies calculated using MSEVB geometries.

the paper. The individual 3-body contributions range from −6.5 to 7.2 kcal/mol. The most favorable 3-body interactions occur for **W1**−**W2**−H_3O^+ and **W3**−**W4**−H_3O^+ in **IV** for which the H-bonding topology is ideally arranged. In contrast, in the **W2**−**W4**−H_3O^+ portion of **I**, the single-donor OH groups of **W2** and **W4** are unfavorably aligned, leading to a positive three-body interaction energy.

The net 4-body interaction energies calculated using the MP2 method range from 0.08 kcal/mol in **II** to 1.19 kcal/mol in **V**, whereas the net 5-body interaction energies are predicted to be 0.1 kcal/mol or less. Thus, to obtain "chemical accuracy" of 1 kcal/mol in describing small protonated water clusters, it is essential to include interactions through fourth order.

We now examine the *n*-body contributions calculated at the Becke3LYP level of theory. The Becke3LYP calculations give net 2-body interaction energies smaller in magnitude by 0.3−2.1 kcal/mol and net 3-body interaction energies 0.1−1.2 kcal/mol less favorable than the MP2 values. The discrepancies between Becke3LYP and MP2 values for the 4- and 5-body interaction energies are less than 0.24 kcal/mol.

The net *n*-body interaction energies calculated using the MSEVB procedure differ appreciably from the MP2 values. The differences are as large as 2.6, 4.7, and 1.9 kcal/mol for the net 2-, 3-, and 4-body interactions, respectively. Particularly striking is the finding that the relaxation energies calculated in the MSEVB procedure are 2.8−5.5 kcal/mol greater than those calculated at the MP2 level. This is due primarily to the H_3O^+ entity rather than the H_2O monomers.

Examination of the individual dimer fragment energies, tabulated in Table 3, reveals that individual $H_3O^+\cdots H_2O$ interaction energies calculated with the MSEVB method differ by 3.7 to −4.6 kcal/mol from the corresponding MP2 values. Moreover, the MSEVB values of the water−water interaction energies differ from the MP2 values by 1.3 to −3.5 kcal/mol. Apparently, the nonrigid TIP3P potential employed in the MSEVB procedure overestimates the attractive interaction between favorably aligned water monomers and is too repulsive for some of the structures with unfavorably aligned dimers.

The trimer fragment interaction energies calculated using the MSEVB procedure differ by 4.0 to −1.8 kcal/mol from the corresponding MP2 values. Again, these differences can be traced in part to deficencies in the TIP3P model.

(iii) Infrared Spectra. The IR spectra of **I**, **II**, **IV**, and **V** calculated in the harmonic approximation and using the Becke3LYP method are summarized in Figure 3. The IR spectrum of **III** is nearly identical to that of **II**, and, thus, is not reported. In discussing the IR spectra, we focus on the OH stretch vibrations which are a particularly sensitive probe of the H-bonding environment.

The IR spectrum of **I** is characterized by an intense triplet of lines at 2747, 2854, and 3008 cm^{-1} due to the three OH stretch modes of the H_3O^+ entity and two less intense lines at 3604 and 3630 cm^{-1} associated with the two single-donor OH groups in the four-membered ring. In **II**, one of the intense transitions associated with the OH stretch modes of the H_3O^+ entity is located at 2358 cm^{-1} and the other two are located at 3032 and 3081 cm^{-1}. The eigenvector associated with the 2358 cm^{-1} vibration is largely localized on the OH group which is H-bonded to the inner-shell **W2** water monomer bound to the second-shell **W4** monomer. The spectrum of **II** also shows an intense transition near 3347 cm^{-1} assocated with the single-donor OH stretch mode of the OH group of the **W2** molecule which is H-bonded to the outer-shell **W4** molecule.

The IR spectrum of **IV** is dominated by two intense lines 2017 and 2278 cm^{-1} associated with OH stretch modes of the H_3O^+ entity and another intense doublet at 3296 and 3313 cm^{-1} due to the single-donor OH groups involved in the H-bonds at the ends of the chain (i.e., **W3** to **W4** and **W2** to **W1**). The vibrations giving rise to the spectral peaks at 2017 and 2278 cm^{-1} are associated with the OH groups of H_3O^+ involved in H-bonds to adjacent H_2O monomers. These are strongly red shifted due to the cooperative effects along the H_3O^+−**W3**−

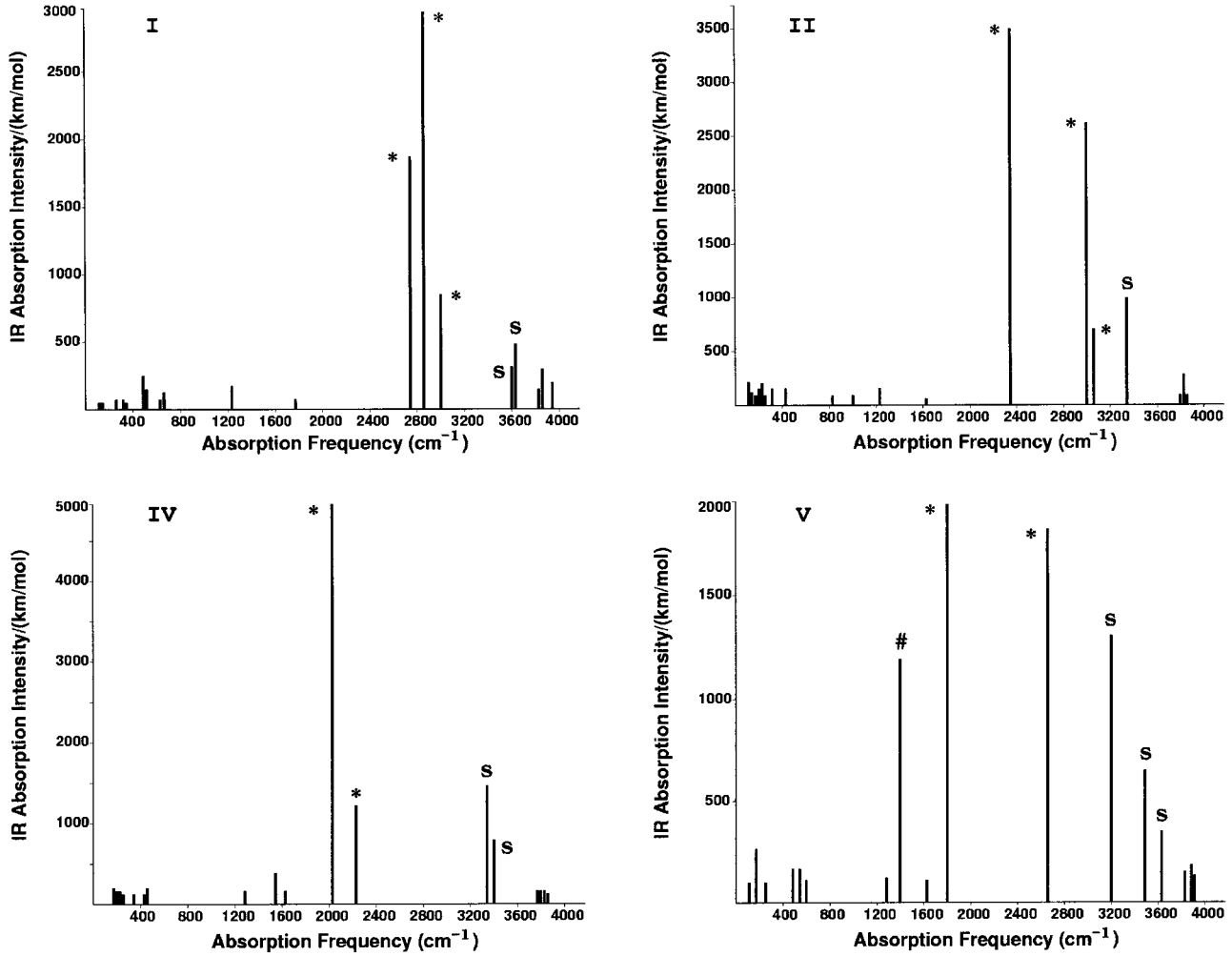

Figure 3. Calculated IR spectra of **I**, **II**, **IV**, and **V**. Results obtained at the Becke3LYP/aug-cc-pVDZ level of theory and employing the harmonic approximation. The symbols * and **S** refer to OH stretch vibrations of the H_3O^+ and single-donor H_2O molecules, respectively. The # symbol denotes bending vibrations with significant admixture of proton transfer coordinate.

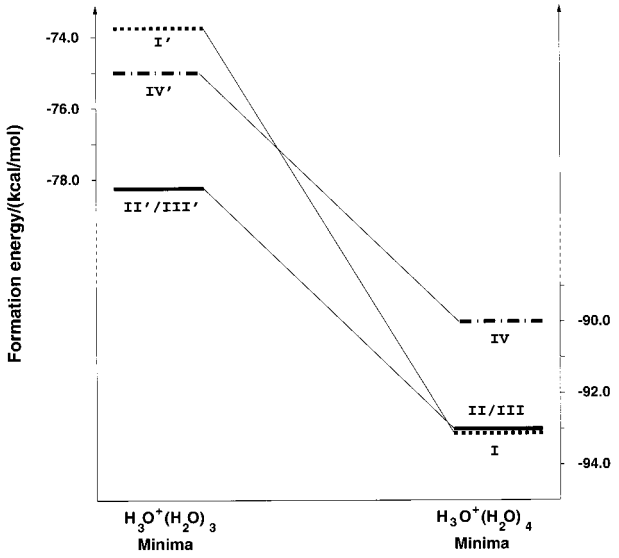

Figure 4. Comparison of the relative energies of the $H_3O^+(H_2O)_4$ and related $H_3O^+(H_2O)_3$ clusters calculated at the MP2/aug-cc-pVDZ level of theory.

W4 and H_3O^+−**W2**−**W1** subunits. The OH stretch vibration associated with the free OH group of the H_3O^+ entity is very weak and is located at 3813 cm^{-1}.

For **V**, the two intense OH transitions at 1797 and 2651 cm^{-1} are due to vibrations associated with the OH groups of H_3O^+ involved in the H-bonding network (the lower frequency mode is due to the OH group of H_3O^+ hydrogen bonded to **W1** and the higher frequency mode to the OH group hydrogen bonded to **W4**). The free OH group of the H_3O^+ entity has a frequency at 3797 cm^{-1} but carries very little intensity. There are also fairly intense lines due to H_2O single-donor OH modes at 3210, 3545, and 3664 cm^{-1}. The intense peak at 1379 cm^{-1} arises from a vibration involving bending motions of H_3O^+ and **W1** and incipient proton transfer between the two molecules.

As noted in the previous section, inclusion of harmonic vibrational zero-point energies destabilizes the various $H_3O^+(H_2O)_4$ isomers by 7.0−9.0 kcal mol^{-1}, with isomer **I** being destabilized the most by this correction (see Table 6). When the vibrational zero-point corrections are added to the MP2-level formation energies, **I**, **II**, and **III** are predicted to be nearly isoenergetic. Clearly, vibrational anharmonicity could be important in determining the relative energies of the various $H_3O^+(H_2O)_4$ isomers.

Figure 5 reports the IR spectra of **I′**, **II′**, and **IV′** calculated in the harmonic approximation and using the Becke3LYP method. Comparison of the calculated spectra of **I** and **I′** and of **II** and **II′** show the expected trends upon adding an extra solvent molecule in going from $H_3O^+(H_2O)_3$ to $H_3O^+(H_2O)_4$. However, the degree of disimiliarity between the spectra of **IV**

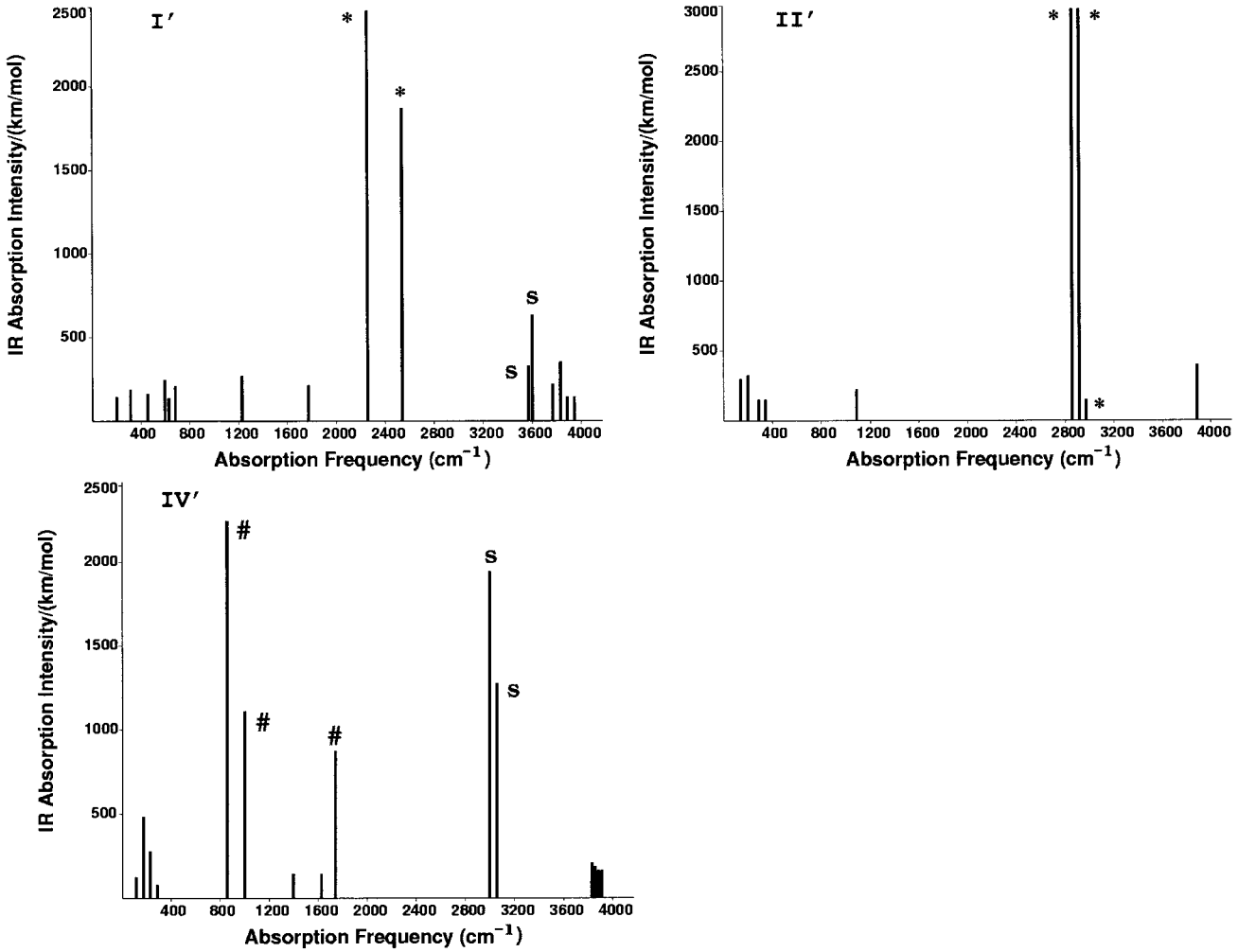

Figure 5. Calculated IR spectra for **I′**, **II′** and **IV′**. Results obtained at the B3LYP/aug-cc-pVDZ level of theory and employing the harmonic approximation. The symbols * and **S** refer to OH stretch vibrations of the H_3O^+ and single-donor H_2O molecules, respectively. The # symbol denotes bending vibrations with significant admixture of proton transfer coordinate.

TABLE 6: Effect of Vibrational ZPE on the Formation Energies (kcal/mol) of the Various $H_3O^+(H_2O)_4$ Isomers

	formation energy	
isomer	without ZPE[a]	with ZPE[b]
I	−92.60	−83.62
II	−91.72	−84.16
III	−91.74	−83.97
IV	−88.47	−81.50
V	−88.60	−80.32

[a] From MP2 calculations using the aug-cc-pVTZ basis set. [b] The vibrational zero-point-energy (ZPE) corrected formation energies were obtained by combining the MP2/aug-cc-pVTZ results with vibrational corrections calculated at the Becke3LYP/aug-cc-pVDZ level of theory and employing the harmonic approximation.

and **IV′** suggests a fundamental difference between the hydrogen bonding topologies in the two structures. Indeed, examination of the geometrical structures reveals that the proton bearing entity in **IV′** is $H_5O_2^+$ rather than H_3O^+ as in **IV** (see Figure 6). In the spectra of **IV′**, the two intense peaks at 3008 and 3061 cm^{-1} are due to OH stretch vibrations associated with the OH groups of the $H_5O_2^+$ entity H-bonded to the two H_2O molecules. The peak at 1729 cm^{-1} arises from an asymmetric bending of the H_2O molecules in $H_5O_2^+$, and the two peaks at 837 and 1013 cm^{-1} correspond to wagging motion of the two hydrogen atoms in $H_5O_2^+$ H-bonded to the **W1** and **W2**

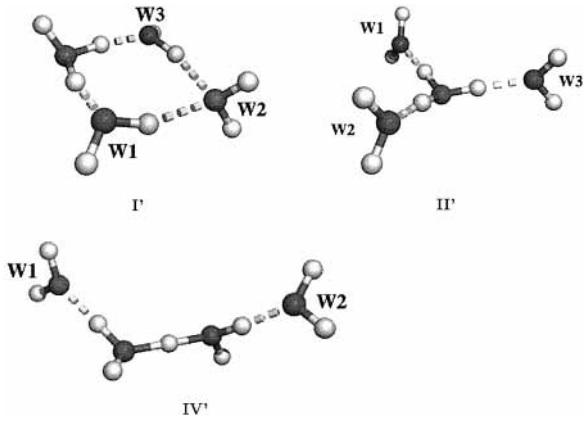

Figure 6. B3LYP/aug-cc-pVDZ optimized geometrical structures of $H_3O^+(H_2O)_3$.

molecules. All three of these vibrations involve significant motion of the central proton in the $H_5O_2^+$ entity.

IV. Conclusions

MP2 level calculations, without inclusion of vibrational zero-point corrections, predict species **I** to be the most stable form of $H_3O^+(H_2O)_4$, with the next most stable isomer lying about 1.2 kcal/mol higher in energy. With the inclusion of vibrational zero-point corrections, the three lowest energy forms of the

cation, **I**, **II** and **III**, are predicted to be almost isoenergetic. Density functional calculations using the Becke3LYP and BP functionals introduce a bias of about 1.1 kcal/mol in favor of structures that lack double-acceptor water monomers compared to those that contain such species. The model potential of Hodges and Stone[17] reproduces the relative energies of the various $H_3O^+(H_2O)_4$ isomers as predicted by the MP2 calculations with a reasonable degree of accuracy. On the other hand, the relative energies calculated using the MSEVB procedure differ by up to 4.5 kcal/mol from the MP2 results. Analysis of the individual 2- and 3-body contributions to the interaction energies reveal that a significant part of the errors in the MSEVB energies can be traced to the use of the TIP3P model to describe the water−water interactions. This suggests that the reliability of this approach could be greatly improved by the adoption of more realistic water−water potentials.

The calculated IR spectra differ appreciably from isomer to isomer, with the OH stretch vibrations of the H_3O^+ species proving to be especially sensitive to the environment of the ion. Comparison of the IR spectra of the $H_3O^+(H_2O)_3$ and $H_3O^+(H_2O)_4$ clusters reveals that for two of the isomers (**I′** → **I** and **II′** → **II**) the introduction of a water monomer in the second solvation shell leads to a large red shift and intensity increase of the OH stretch vibration associated with the OH group of H_3O^+ directly involved in the "extended" H-bonding network. On the other hand, the chainlike forms of $H_3O^+(H_2O)_3$ and $H_3O^+(H_2O)_4$ are found to be fundamentally different, with the proton being associated with a $H_5O_2^+$ entity in the former and with a H_3O^+ entity in the latter.

Acknowledgment. We thank Udo Schmitt for helpful discussions about the MSEVB method. The calculations were carried out on the IBM 43P 260 computers in the University of Pittsburgh's Center for Molecular and Materials Simulations. These computers were funded by grants from NSF and IBM.

References and Notes

(1) Newton, M. D.; Ehrenson, S. *J. Am. Chem. Soc.* **1971**, *93*, 4971.
(2) Newton, M. D. *J. Chem. Phys.* **1977**, *67*, 5535.
(3) Diercksen, G. H. F.; Kramer, W. P.; Roos, B. O. *Theor. Chim. Acta* **1975**, *36*, 249.
(4) Scheiner, S. *J. Am. Chem. Soc*. **1981**, *103*, 315.
(5) Stillinger, F. H.; David, C. W. *J. Chem. Phys.* **1978**, *69*, 1473.
(6) Halley, J. W.; Rustad, J. R.; Rahman, A. *J. Chem. Phys.* **1993**, *98*, 4110.
(7) Kozack, R. E.; Jordan, P. C. *J. Chem. Phys.* **1993**, *99*, 2978.
(8) Ojamäe, L.; Shavitt, I.; Singer, S. J. *Int. J. Quantum Chem.* **1995**, *29*, 657.
(9) Ojamäe, L.; Shavitt, I.; Singer, S. J. *J. Chem. Phys.* **1998**, *109*, 5547.
(10) Vuilleumier, R.; Borgis, D. *J. Mol. Struct.* **1997**, *436*, 555.
(11) Vuilleumier, R.; Borgis, D. *Chem. Phys. Lett.* **1998**, *284*, 71.
(12) Valeev, E. F.; Schaefer, H. F. *J. Chem. Phys*. **1998**, *108*, 7197.
(13) Tuckerman, M.; Laasonen, K.; Sprik, M.; Parinello, M. *J. Chem. Phys.* **1995**, *103*, 150.
(14) Sagnella, D. E.; Tuckerman, M. E. *J. Chem. Phys.* **1998**, *108*, 2073.
(15) Wei, D.; Salahub, D. R. *J. Chem. Phys.* **1994**, *101*, 7633.
(16) Schmitt, U. W.; Voth, G. A. *J. Chem. Phys*. **1999**, *111*, 9361.
(17) Hodges, M. P.; Stone, A. J. *J. Chem. Phys.* **1999**, *110*, 6766.
(18) Corongiu, G.; Kelterbaum, R.; Kochanski, E. *J. Phys. Chem*. **1995**, *99*, 8038.
(19) Geissler, P. L.; Dellago, C.; Chandler, D. *Phys. Chem. Chem. Phys.* **1999**, *1*, 1317.
(20) Geissler, P. L.; Dellago, C.; Chandler, D.; Hutter, J.; Parrinello, M. *Chem. Phys. Lett.* **2000**, *321*, 225.
(21) Eigen, M.; Maeyer, L. D. *Proc. R. Soc. A.* **1958**, *247*, 505.
(22) Becke, A. D. *Phys. Rev. A* **1988**, *38*, 3098.
(23) Perdew, J. P. *Phys. Rev. B* **1986**, *33*, 8822.
(24) Perdew, J. P. *Phys. Rev. B* **1986**, *38*, 7406.
(25) Kim, K.; Jordan, K. D. *J. Phys. Chem.* **1994**, *98*, 10 089.
(26) Sim, F.; St.-Amant, A.; Papai, I.; Salahub, D. R. *J. Am. Chem. Soc.* **1992**, *114*, 4391.
(27) Laasonen, K.; Csajka, F.; M. P. *Chem. Phys. Lett.* **1992**, *194*, 172.
(28) Laasonen, K.; Parinello, M.; Car, R.; Lee, C.; Vanderbilt, D. *Chem. Phys. Lett.* **1993**, *207*, 208.
(29) Becke, A. D. *J. Chem. Phys.* **1993**, *98*, 5648.
(30) Lee, C.; Yang, W.; Parr, R. *Phys. Rev. B* **1993**, *37*, 785.
(31) Frisch, M. J.; Trucks, G. W.; Schlegel, H. B.; Scuseria, G. E.; Robb, M. A.; Cheeseman, J. R.; Zakrzewski, V. G.; Montgomery, J. A., Jr.; Stratmann, R. E.; Burant, J. C.; Dapprich, S.; Millam, J. M.; Daniels, A. D.; Kudin, K. N.; Strain, M. C.; Farkas, O.; Tomasi, J.; Barone, V.; Cossi, M.; Cammi, R.; Mennucci, B.; Pomelli, C.; Adamo, C.; Clifford, S.; Ochterski, J.; Petersson, G. A.; Ayala, P. Y.; Cui, Q.; Morokuma, K.; Malick, D. K.; Rabuck, A. D.; Raghavachari, K.; Foresman, J. B.; Cioslowski, J.; Ortiz, J. V.; Stefanov, B. B.; Liu, G.; Liashenko, A.; Piskorz, P.; Komaromi, I.; Gomperts, R.; Martin, R. L.; Fox, D. J.; Keith, T.; Al-Laham, M. A.; Peng, C. Y.; Nanayakkara, A.; Gonzalez, C.; Challacombe, M.; Gill, P. M. W.; Johnson, B. G.; Chen, W.; Wong, M. W.; Andres, J. L.; Head-Gordon, M.; Replogle, E. S.; Pople, J. A. *Gaussian 98*, revision A.7; Gaussian, Inc.: Pittsburgh, PA, 1998.
(32) del Bene, J. E.; Frisch, M. J.; Pople, J. A. *J. Phys. Chem.* **1985**, *89*, 3669.
(33) Brooks, B. R.; Bruccoleri, R. E.; Olafson, B. D.; States, D. J.; Swaminathan, S.; Karplus, M. *J. Comput. Chem.* **1983**, *4*, 1987.
(34) Dunning,T. H. *J. Chem. Phys.* **1989**, *90*, 1007.
(35) Kendall, R. A.; Dunning, T. H.; Harrison, R. J. *J. Chem. Phys*. **1992**, *96*, 6796.
(36) Boys, S. F.; Bernardi, F. *Mol. Phys*. **1970**, *19*, 553.
(37) Pedulla, J. M.; Kim, K.; Jordan, K. D. *Chem. Phys. Lett*. **1998**, *291*, 78.
(38) Xantheas, S. S. *J. Chem. Phys.* **1996**, *104*, 8821.